Technical Report No.: USC-VacUV-101

15 June 1965

Contract NsG-178-61 on

Vacuum Ultraviolet and Solid State Physics

FAR ULTRAVIOLET RESPONSE OF SILICON P-N JUNCTION PHOTODIODES

by

A. L. Morse, W.F. Crevier, and G.L. Weissler
University of Southern California

and

D. B. Medved
Electro-Optical Systems, Inc., Pasadena

Submitted by

G. L. Weissler, Chief Investigator
Contract No. NsG-178-61

Prepared for

Office of Grants and Research Contracts
National Aeronautics and Space Administration
Washington, D.C. 20546

TABLE OF CONTENTS

LIST OF FIGURES

LIST OF TABLES

ABSTRACT

The responsivity Q' of silicon p-n junction photodiodes has been measured from 2000 to 500Å ($h\nu$ = 6 to 25 eV). The value of Q' (effectively the product of quantum yield Q and pair collection efficiency C) for a shallow junction (0.3μ) diode decreases slightly from a value of 0.4 to 0.2 in the range 6 to 18 eV and then rises sharply to 1.4 at 25 eV. The use of the device as a solid state detector in the far ultraviolet is discussed.

I. INTRODUCTION

The optical properties of semiconductors have been studied by various investigators in the middle and extreme uv,[1-4] and the connection between these measurements and the electron energy band structure has been extensively discussed.[5-8] Recently, Tuzzolino investigated the electrical consequences of high energy photon absorption from a device standpoint[9] and as part of a fundamental study of impact ionization[10] using a silicon surface-barrier diode. He found internal quantum efficiencies in silicon of the order

---

[1] H. R. Philipp and E. A. Taft, Phys. Rev. 120, 37 (1960).

[2] T. Sasaki and K. Ishiguro, Japan. J. Appl. Phys. 2, 289 (1963).

[3] Om P. Rustgi, J. S. Nodvik, and G. L. Weissler, Phys. Rev. 122, 1131 (1961).

[4] H. R. Philipp and H. Ehrenreich, Phys. Rev. 129, 1550 (1963).

[5] J. C. Phillips, Phys. Rev. 125, 1931 (1962).

[6] H. Ehrenreich, H. R. Philipp, and J. C. Phillips, Phys. Rev. Letters 8, 59 (1962).

[7] E. Loh and J. C. Phillips, J. Chem. Phys. Solids 24, 495 (1963).

[8] J. C. Phillips, Phys. Rev. 133, A452 (1964).

[9] A. J. Tuzzolino, Rev. Sci. Instr. 35, 1332 (1964).

[10] A. J. Tuzzolino, Phys. Rev. 134, A205 (1964).

of $Q \simeq 15$ electrons per absorbed photon at $h\nu = 21.2$ eV. The use of the surface-barrier diode either directly or in combination with sodium salicylate as a vacuum uv detector was discussed. At 1216Å he computed the minimum detectable rms photon flux to be $N' = 2.5 \times 10^6$ photons per second.

In this paper, the responsivity of a p-n junction photodiode in the vacuum ultraviolet is discussed. This device requires no external bias for operation, and it has a dark current lower than 10^{-12}A compared to about 10^{-8}A for the surface-barrier diode. Although the collection efficiency of the junction device turns out to be only about 5 to 10 per cent of a surface barrier configuration at 1000Å, the shot noise is roughly 100 times lower. It is estimated that the minimum detectable photon flux is about 10^6 photons/sec.

II. SPECTRAL RESPONSE OF JUNCTION DEVICES

A. Qualitative Discussion

The wavelength dependence of the response of p-n junction devices is determined by an interplay of several mechanisms. These involve primarily

a) the absorption of the incident radiation with the consequent generation of hole-electron pairs for the case where the condition $h\nu > E_g$ is met. E_g is the bandgap energy and ν the frequency of the incident radiation;

b) the transport of the carriers thus produced by means of diffusion and/or drift in an electric field to a p-n junction, where they are separated by the junction field to generate an external voltage or current. Equations governing the interplay of such mechanisms have been developed as part of a general analytic framework. A qualitative discussion follows.

Consider the absorption coefficient as a function of wavelength for silicon[1] shown in Fig. 1. The absorption threshold corresponds to a bandgap of 1.1 eV. A simplified band structure of silicon[7] is shown in Fig. 2, and the phonon-assisted transition corresponding to the absorption threshold is labeled T_i. Silicon is an indirect semiconductor. The transition probabilities are lower for these indirect transitions of type T_i than they are for a direct transition T_d. Thus, the absorption coefficient between the indirect threshold of 1.1 eV and the direct threshold of 3.4 eV rises at a much slower rate than the sharp increase which occurs above 3.4 eV for $\lambda < 3600$Å. It is assumed throughout this discussion that

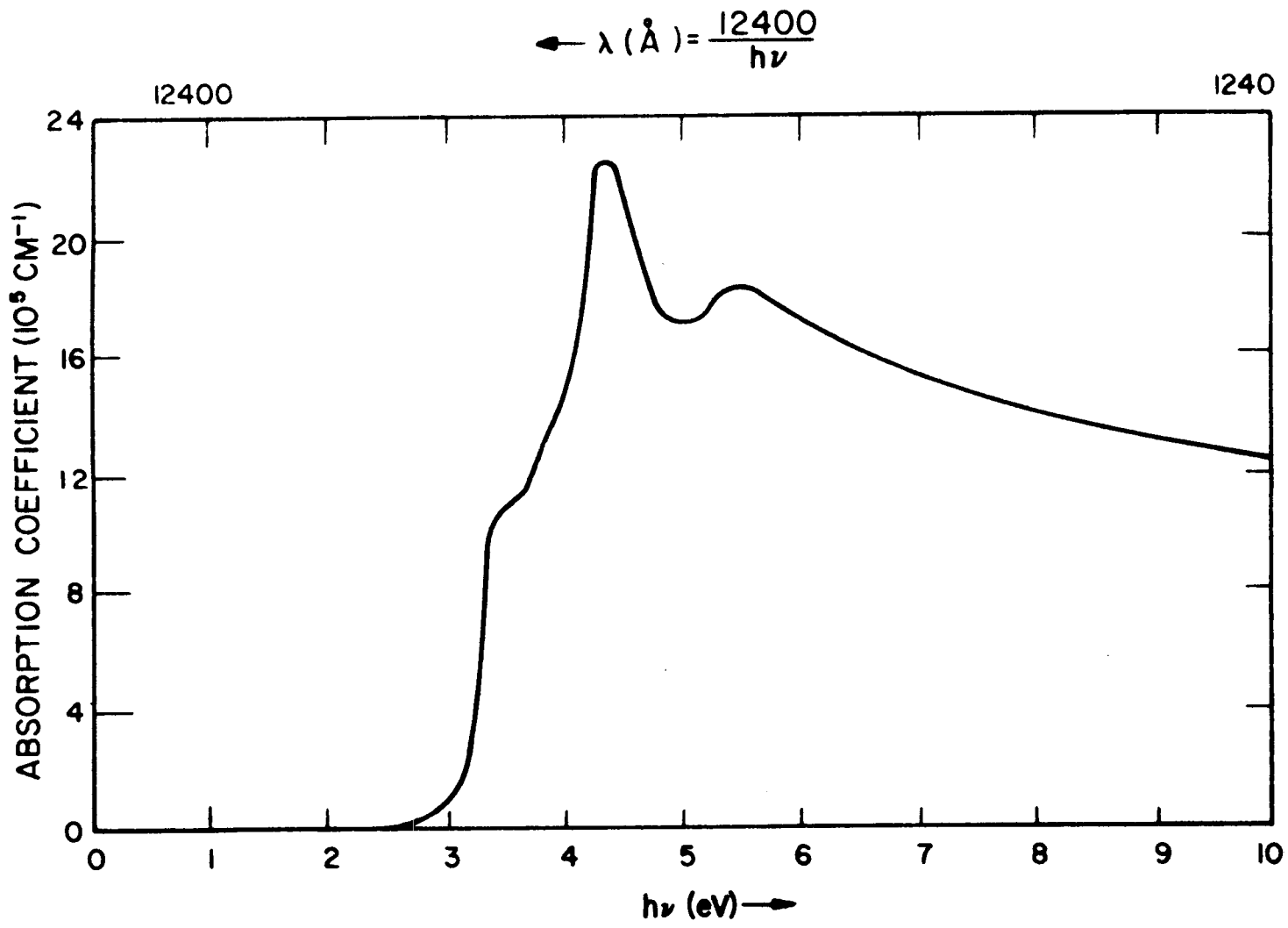

Fig. 1. Absorption Coefficient of Silicon as a Function of Wavelength

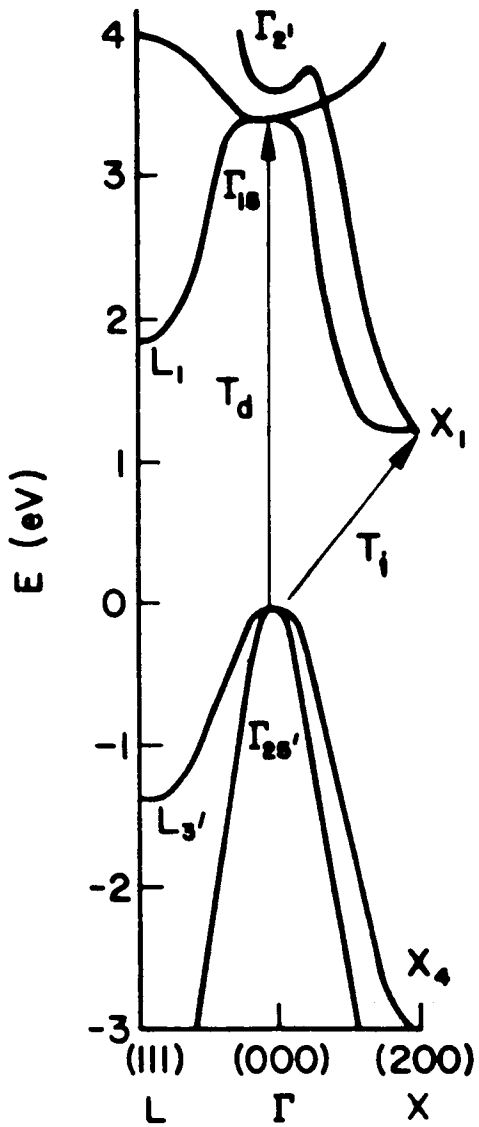

Fig. 2. Energy Band Structure of Silicon (For explanation of symbols not used in the text, see ref. 7).

the quantum efficiency for pair production is effectively unity and wavelength independent. It will turn out that this assumption breaks down at the shorter wavelengths, where secondary pair production resulting from the generation of sufficiently energetic carriers may occur (see discussion in Section V).

The detectivity, D^*_λ, of a typical p-n junction diode is shown in Fig. 3, curve A. The spectral detectivity D^*_λ is defined as

$$D^*_\lambda = \frac{\sqrt{A\ \Delta f}}{NEP} , \qquad (1)$$

where A is the area of the device, Δf is the electrical bandwidth, and NEP is the noise-equivalent power. The units of D^*_λ are thus $cm(sec)^{-\frac{1}{2}}watt^{-1}$. If the signal-to-noise ratio varies as the reciprocal of the square root of the device area, the D^*_λ parameter is area-insensitive. The variation in detectivity can be explained with reference to Fig. 4, which shows a plane at the mean depth of carrier generation. On this plane the radiation intensity has decreased by a factor of 1/e from its incident value. The general distance, thus defined, is the reciprocal of the absorption coefficient for a homogenous material. The maximum of the detectivity curve (region 2 of Fig. 3) thus corresponds to a condition where the carrier generation distance and diffusion length L_n are such that a maximum number of carriers will reach the junction. At longer wavelengths, region 1 corresponds to the condition where most carriers are produced deep in the bulk of the material (low absorption coefficient) at distances in excess of their diffusion length. On the other

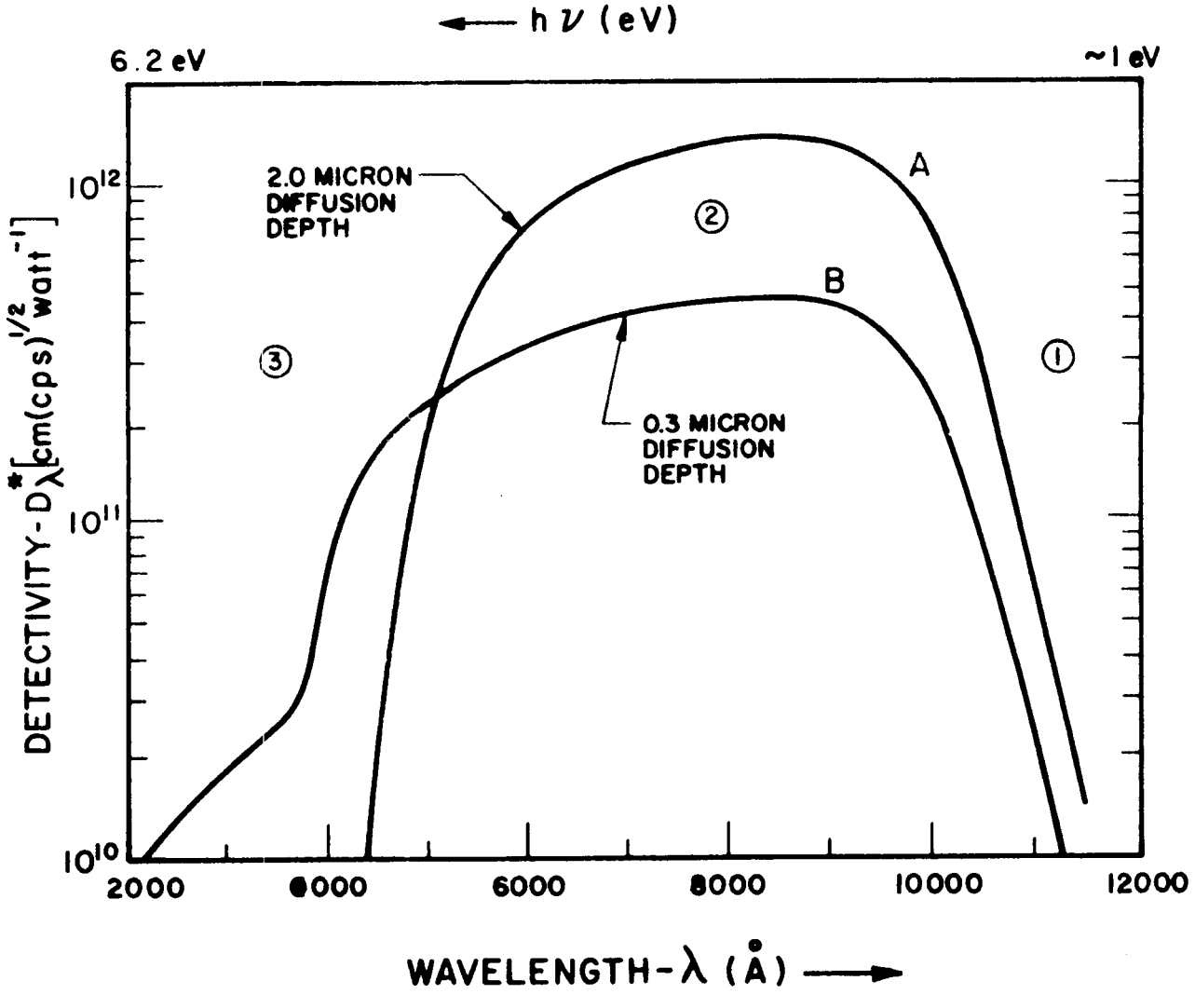

Fig. 3. Spectral Responsivity of Typical Silicon Junction Devices

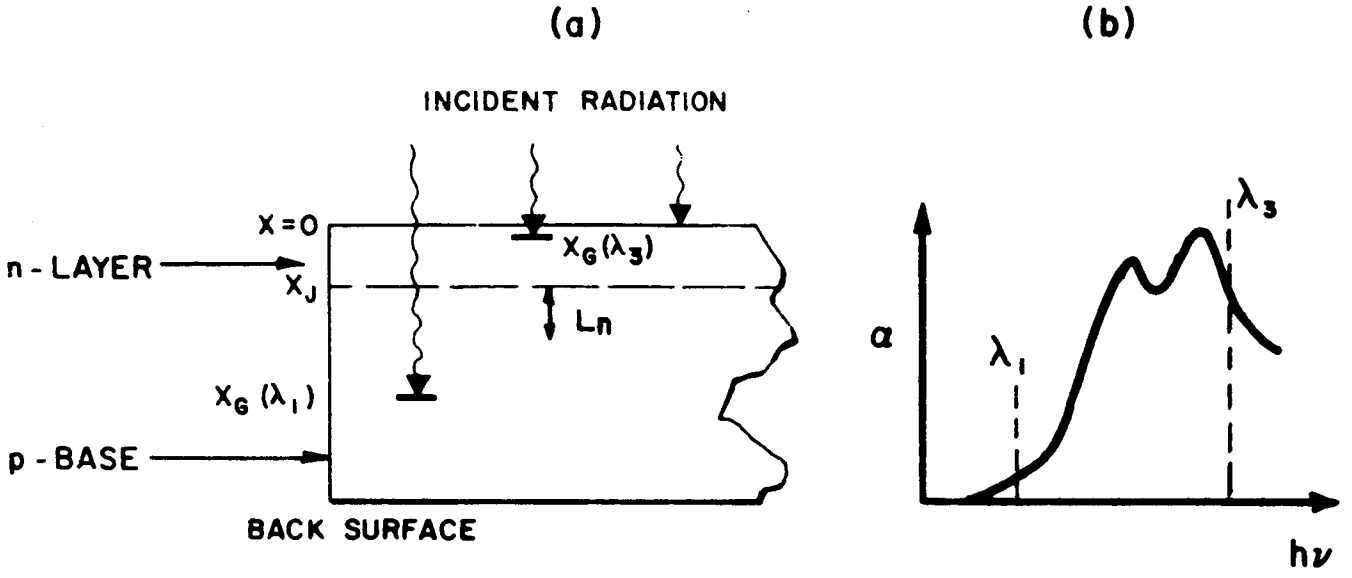

X = 0, SURFACE EXPOSED TO LIGHT

X_J = DISTANCE OF JUNCTION PLANE FROM IRRADIATED SURFACE

$X_G(\lambda_1)$ = DISTANCE BELOW SURFACE FOR GENERATION OF HOLE-ELECTRON PAIRS AT WAVELENGTH λ_1

$X_G(\lambda_3)$ = DISTANCE BELOW SURFACE FOR GENERATION OF HOLE-ELECTRON PAIRS AT WAVELENGTH λ_3

Abs. COEFFICIENT, α, VARIATION WITH PHOTON ENERGY

$\lambda_3 < \lambda_{max} < \lambda_1$

AND $\alpha_3 >> \alpha_1$

Fig. 4. Absorption Depths of Light in Silicon at Different Wavelengths

hand, the sharp drop-off in sensitivity for region 3 results from absorption of the photons very close to the surface. The surface acts as a recombination sink, with the lifetime of the carriers much less than that in the bulk. Correspondingly, a smaller fraction of the carriers that are generated will reach the junction before recombination occurs. The region of maximum detectivity can be qualitatively stated by the expression

$$x_J + L_n = \frac{1}{\alpha(\lambda \text{ max})} . \tag{2}$$

It is apparent that the short wavelength response would be increased if shallower junctions than those shown were used (see, for example, curve B of Fig. 3).

B. Mathematical Formulation

The equation governing production, diffusion, and recombination of minority carriers resulting from photon absorption is

$$D \frac{d^2n}{dx^2} - \frac{n}{\tau} + \int_0^{\lambda} N(\lambda)\alpha(\lambda)e^{-\alpha x} \, d\lambda = 0. \tag{3}$$

D is the diffusion coefficient and n(x) is the excess minority carrier concentration produced by photon absorption in the p-region (correspondingly, p(x) is used in the n-region). The second term is the recombination rate determined by the minority carrier lifetime τ. The third term is the production rate, written for the general case of all wavelengths with distribution in photon flux $N(\lambda)$ and absorption coefficient $\alpha(\lambda)$.

For the case of monochromatic light incident on a junction diode, $N(\lambda)$ becomes N_λ (the flux density in photons/(cm^2 sec) at wavelength λ_o), yielding

$$D \frac{d^2n}{dx^2} - \frac{n}{\tau} + N_\lambda \alpha_\lambda e^{-\alpha x} = 0 \qquad (3a)$$

subject to the boundary conditions

$$n(x_J) = 0 \qquad (4)$$

and

$$n(\infty) = 0. \qquad (5)$$

The internal collection efficiency, C, is defined to be the ratio of the number of carriers produced by the absorbed photons to the number separated at the junction. Van Roosbroeck[11] has solved the small signal equation (3) for contributions from both sides of the junction and found that in the limit of $(\alpha L_s)^{-1} << 1$

$$C = \frac{2(1 + S/\alpha L_s)}{(S + 1)\exp(x_J/L_s) - (S - 1)\exp(-x_J/L_s)}, \qquad (6)$$

where

$$S = \frac{sL_s}{D_o},$$

and L_s = the diffusion length corresponding to recombination in the surface layer,

s = surface recombination velocity, and

D_o = small signal ambipolar diffusivity.

No attempt has been made to match these solutions with the

---

[11] W. G. Pfann and W. van Roosbroeck, J. Appl. Phys. 25, 1422 (1954).

data on the photodiodes used in these experiments. There is too much uncertainty concerning the magnitude of such parameters as the surface recombination velocity, internal electric field profiles from the surface to the junction, device lifetime, etc. Such a direct comparison may be made after careful study of these questions. For most of the purposes of this report, it is sufficient to use the qualitative model for prediction and interpretation of the observed spectral responsivity.

III. DIODE FABRICATION AND STRUCTURE

The fabrication technology used was adapted from standard transistor methods[12,13] outlined in Table I. There are two separate n-impurity diffusions. Both the guard ring and the deep (2.5μ) peripheral regions are formed during the first higher temperature diffusion. The active region (center area) is formed during the second diffusion.

The SiO_2 layer formed during the diffusions is selectively etched away from the photosensitive and contact areas.

The contact areas are coated with a thin layer of aluminum that is partially alloyed into the silicon.

After scribing, the diodes are eutectically bonded onto a transistor header. Contact is made by thermocompression, bonding 0.001 inch gold wire to the aluminized areas and to the insulated pins.

Fig. 5 shows top and cross section views of the photodiodes. Fig. 6 is a photomicrograph of a diode which has been beveled and stained to make visual the relative diffusion depth of the p-n junction. Fig. 7 shows a completed diode mounted on a TO-5 transistor base.

An important parameter in determining D^*_λ and one which is also dependent on processing, is the reverse leakage current.

---

[12] D. B. Medved, Final Report on Contract AF 33(675)-29144, Electro-Optical Systems, Inc., Pasadena, Technical Report No. 4651F, July 1964.

[13] L. Garasi, S. Kaye, and D. B. Medved, Electro-Optical System, Inc., Pasadena, Internal Report, June 1964.

TABLE I

PROCEDURE FOR PHOTODIODE FABRICATION

1. Polish etch silicon p-type crystal.
2. Oxidize.
3. Photoresist mask and etch oxide over contact and guard ring areas.
4. Diffuse phosphorous into contact and guard ring areas to a depth of 2.5μ.
5. Photoresist mask and etch oxide over light-sensitive and contact areas.
6. Diffuse phosphorous into photosensitive area to a depth of 0.5μ.
7. Photoresist mask and etch oxide over light-sensitive and contact areas.
8. Evaporate aluminum.
9. Photoresist mask and etch aluminum over contact areas.
10. Alloy aluminum.
11. Mount on header and attach leads.

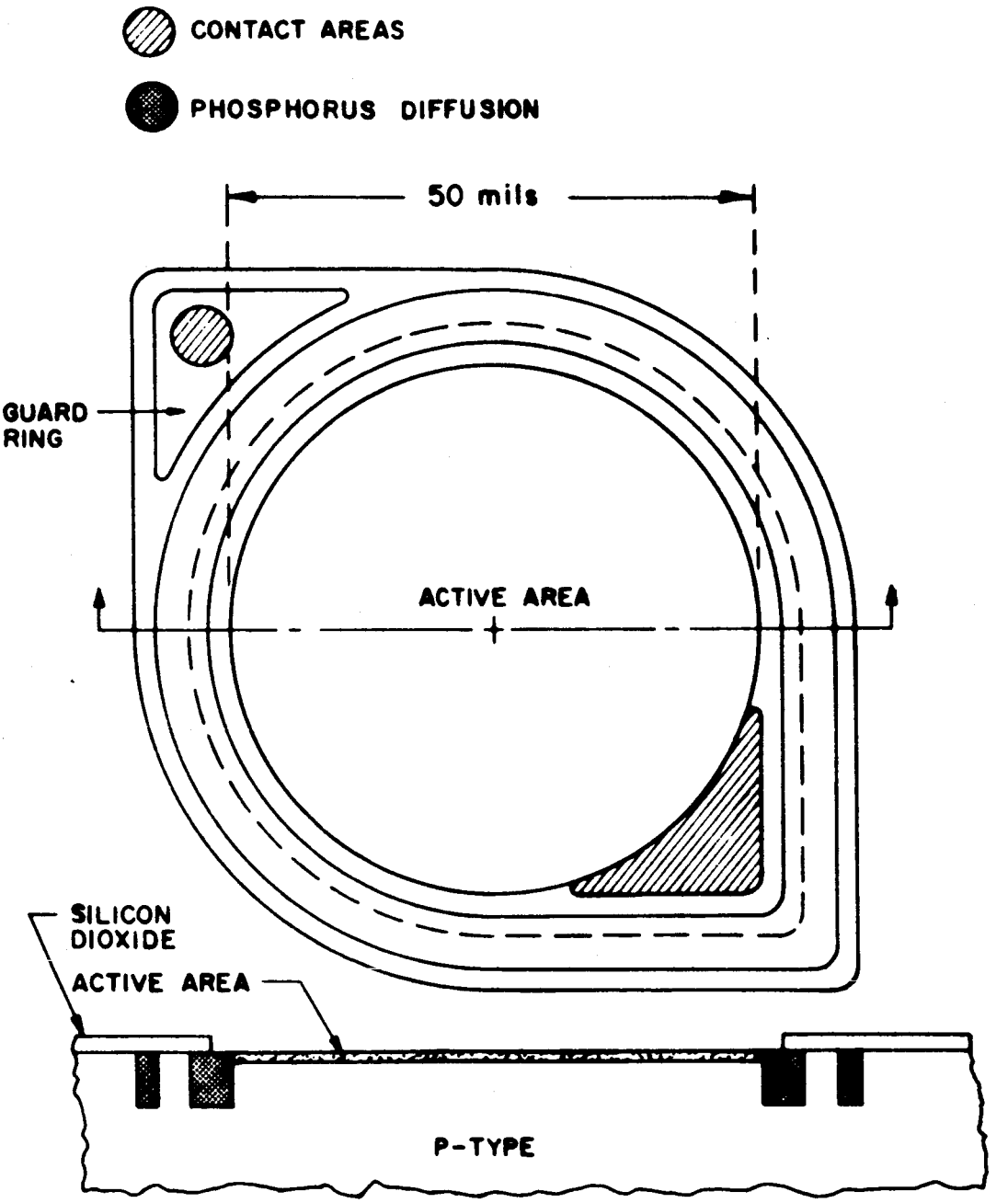

Fig. 5. Diode Configuration

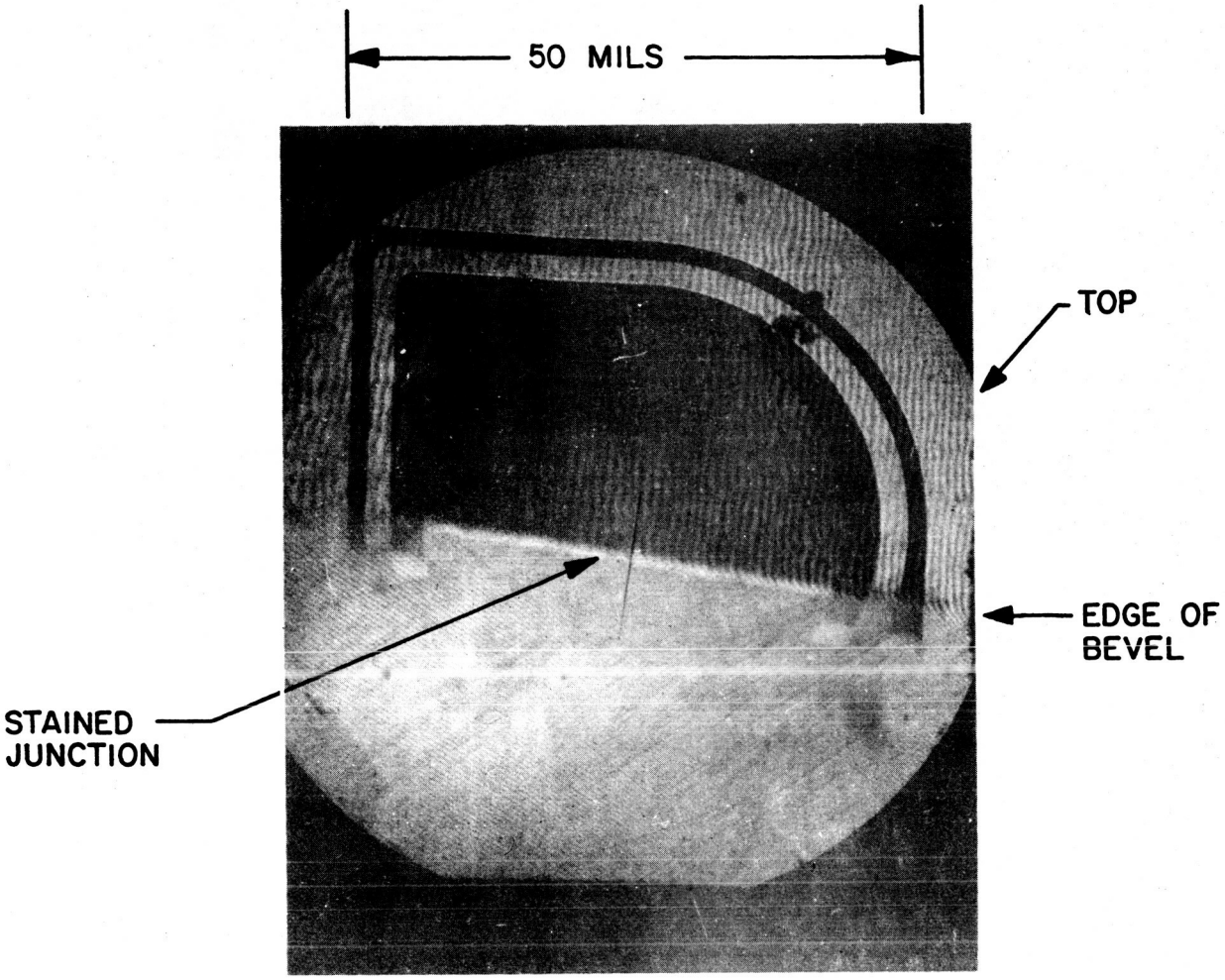

Fig. 6. Beveled Photodiode

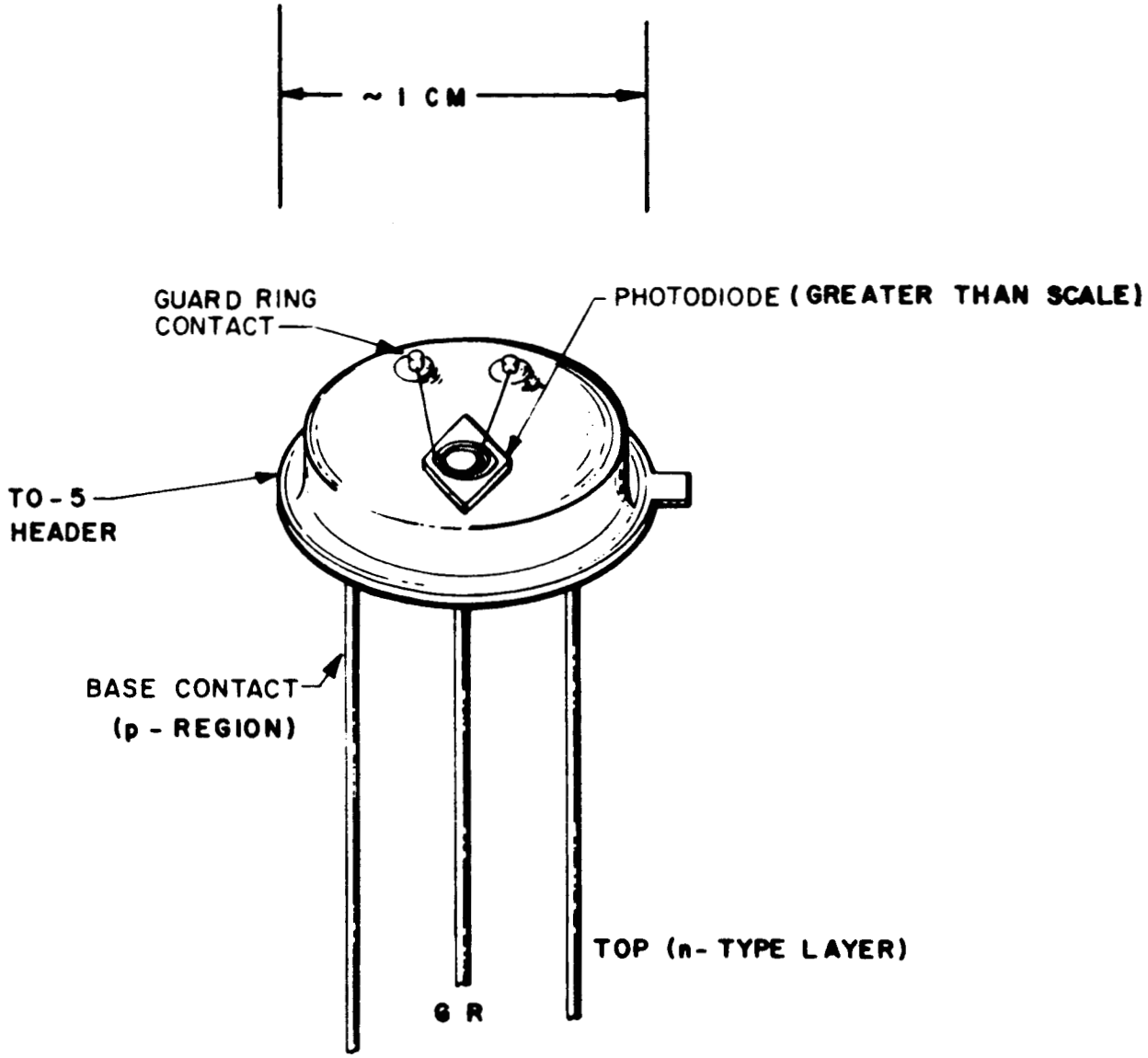

Fig. 7. Photodiode Mounted on Header

Unfortunately, as the base resistivity is increased, surface leakage also increases. The best solution appears to be the use of a guard ring.

The diffusion of phosphorous into a p-type (boron-doped) base produces a profile such as shown in Fig. 8.

The diffusion profiles are described by the complementary error function

$$N_D(x) = N_D(0)\ \text{erfc}\ \frac{x}{2\sqrt{Dt}}\ , \tag{7}$$

where $N_D(0)$ is the surface concentration and t is the time of diffusion. The diffusion coefficient, D, is assumed to be independent of concentration. The distribution of Eq. (7) results with diffusion occurring under conditions where $N_D(0)$ is held constant. A Gaussian distribution results if the total impurity used in the diffusion is kept constant. A tabulation of the average conductivity, $\bar{\sigma}$, as a function of surface concentration with thickness of the diffused layer is given by Irvin,[14]

$$\bar{\sigma} = \frac{1}{x_J}\int_0^{x_J} q\mu\ N_D(x)dx. \tag{8}$$

For the diodes of this report, $N_D(0) \geq 10^{20}/cm^3$ and $x_J = 0.3\mu$.

---

[14] J. C. Irvin; Bell Laboratories Monograph 4092.

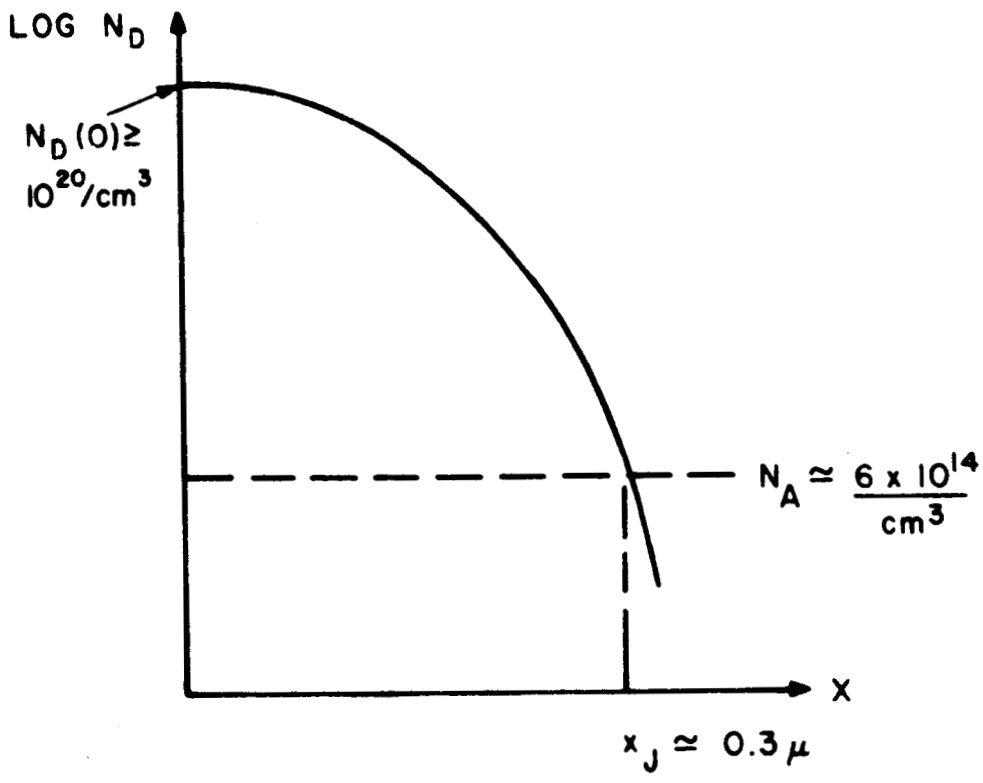

Fig. 8. Diffusion Profile. N_D is the donor concentration, N_A is the accepter concentration, and x_j is the depth where these two are equal.

IV. APPARATUS

A one-meter, normal incidence vacuum monochromator[15] was used to irradiate the various detectors with monochromatic radiation. The instrument, shown in Fig. 9, was originally a spectrograph but was converted to a monochromator by mounting the aluminum grating in a holder which could be rotated about its vertical axis. As the grating turned, various spectral lines moved across the exit slit, covering a spectral region from 3500 to 425Å in the first order. The long wavelength limit was due to serious defocusing when the grating was turned through large angles, while the lower limit was determined by the low reflectance of aluminum near normal incidence.

Two light sources were used. One, with a dc voltage of 750V and a current of 0.4A, was a time-continuous glow discharge through a water-jacketed quartz capillary tube. A glow discharge through air at a pressure of about one torr created lines between 3300 and 1600Å which were too weak to provide a clear signal in the thermopile radiation detector; however, at least 15 of them were easily detected with the silicon photodiodes. A hydrogen discharge produced the strongest spectral lines and covered the region from 1624 to 1024Å. The photodiodes gave a good response to 25 lines in this region, and twelve of them were intense enough to provide a signal from the thermopile. Helium in the

---

[15] G. L. Weissler, Handbuch der Physik (Berlin: Springer-Verlag, 1956), Vol. XXI, p. 317

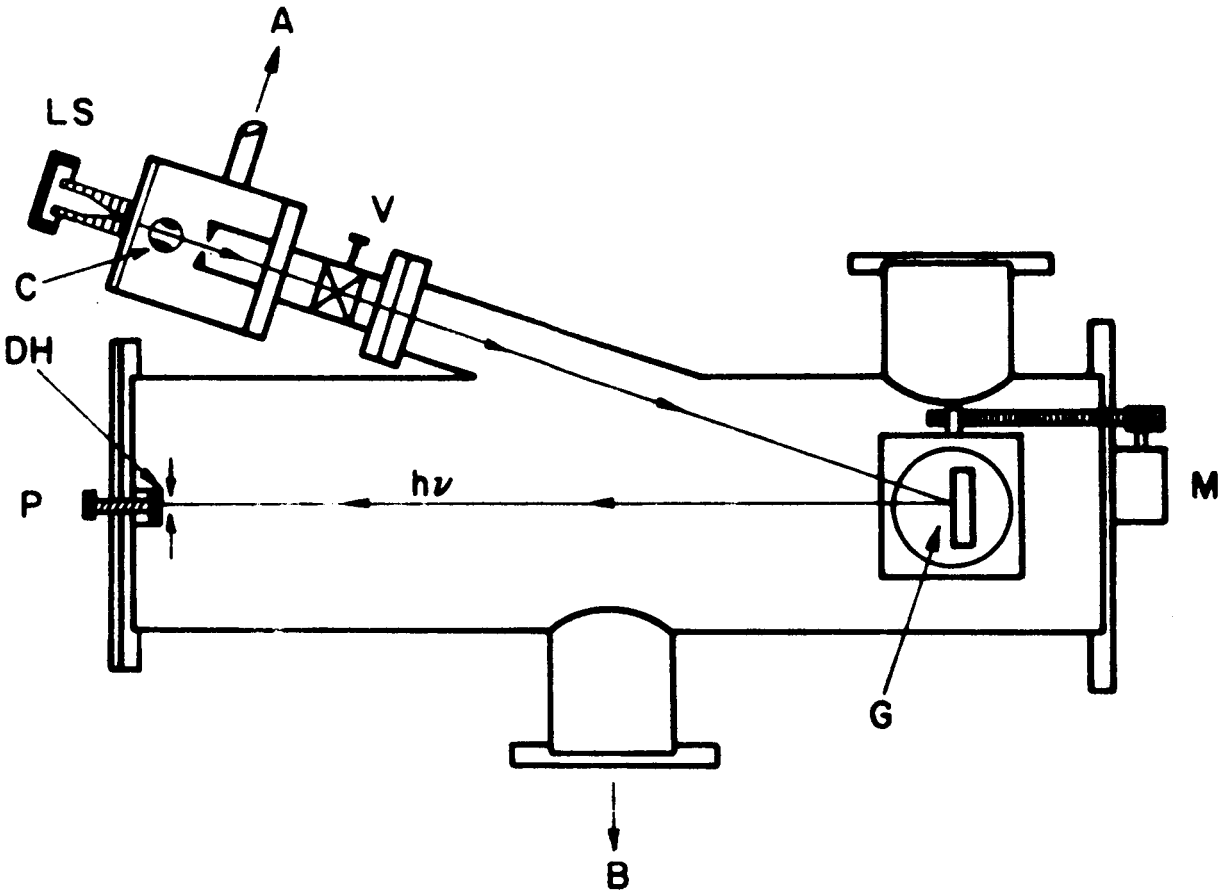

Fig. 9. One-Meter Normal Incidence Monochromator

A: To roughing pump for light source;
B: To diffusion pump for main chamber;
C: Mechanical light chopper;
DH: Detector holder and electron suppressor plate;
G: Grating and grating holder;
LS: Light source;
M: Motor and gear assembly for grating drive;
P: Extension of pinion through the chamber wall;
V: Valve.

dc discharge gave rise to a strong line at 584Å.

The second source was a condensed spark discharge through a ceramic capillary filled with air at about 50μ. At 8 kV the average discharge current was 32 mA. The discharge capacitor was 0.04 μF, and the discharge rate was 90 sparks/sec. Several air spark spectra will be shown later.

The radiation from the source was chopped at 11 cps by a rotating cylinder placed between the light source and the entrance slit. The cylinder, which spun about its vertical axis, had a slot in it which passed radiation twice every revolution, and the size of the slot was such that the light was on and off for equal amounts of the time. The cylinder was coupled magnetically to a motor outside the vacuum chamber.

A Bausch and Lomb, one-meter radius of curvature, concave, aluminum grating was used to disperse the radiation. It was ruled with 1440 grooves/mm over an area of 5 x 3 cm^2. A normal scanning speed of approximately 75Å/min was used with this grating.

The two silicon photodiodes evaluated in this work and a thermopile radiation detector* were mounted in an aluminum block which could be moved vertically up and down by a rack and pinion, as shown in Fig. 10. The pinion was turned by a shaft which extended through the vacuum wall. An exit slit, mounted on an insulated electron suppressor plate, was placed in front of the detector holder. Both the exit and entrance slits were 3 x 0.5 mm^2

*Manufactured by Charles M. Reader and Co., Detroit, Mich., Model No. RUV-8VC.

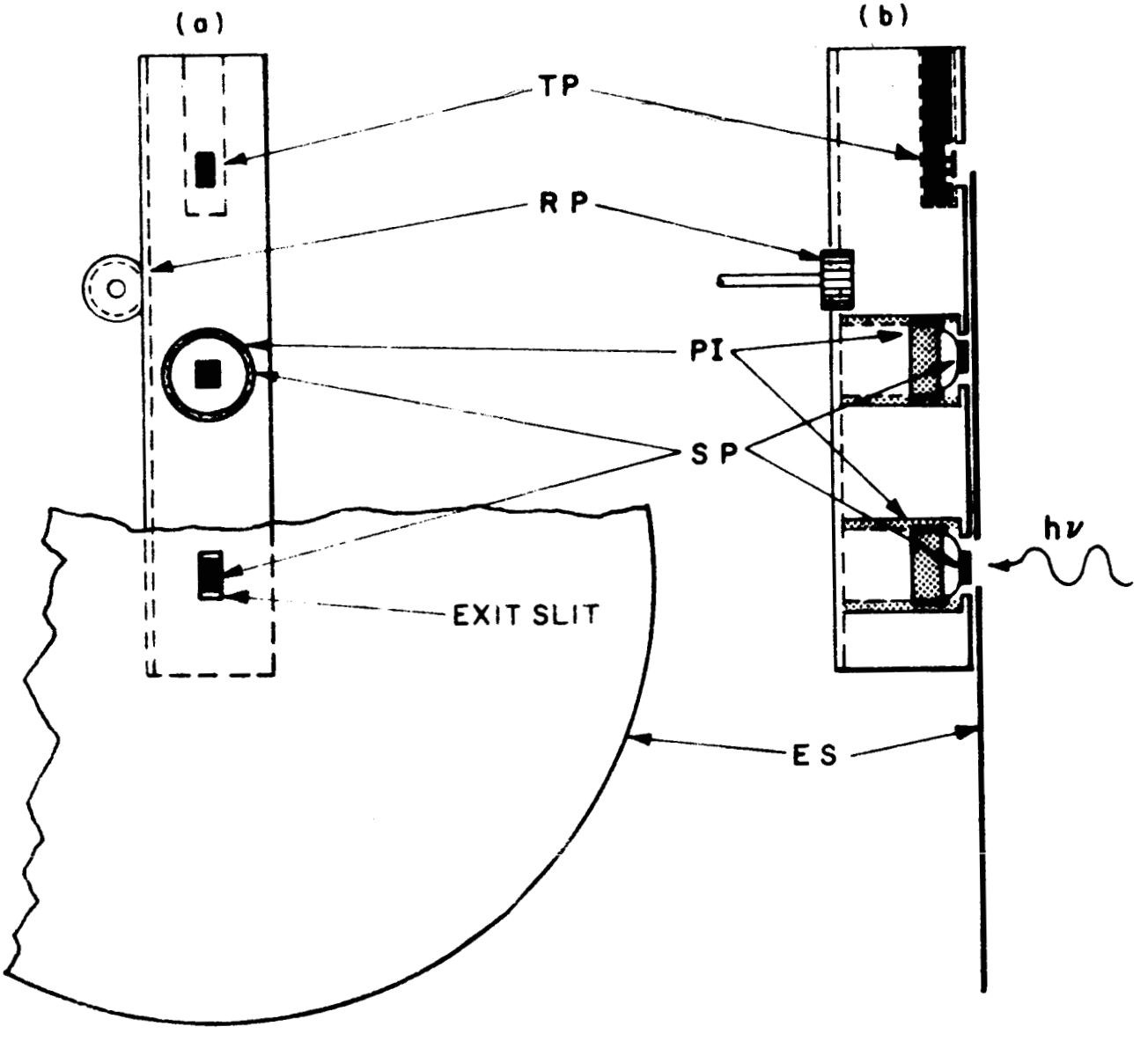

Fig. 10. Detector Holder and Electron Suppressor Plate

TP: Thermopile;
RP: Rack and pinion used to raise and lower the detectors
PI: Plastic insulators between the diodes and the holder;
SP: Silicon photodiodes;
ES: Electron suppressor plate.

in area. A width of 0.5 mm corresponded to a radiation bandwidth of 8Å.

As seen in Fig. 11, there were three leads from each diode.* One was connected to the n-side of the junction which was exposed to the radiation. The lead to the unexposed p-side of the junction was also connected to the metal case of the diode. To permit the p-side to be isolated from ground, it was necessary to use a plastic insulator between the case and the grounded aluminum holder. The lead marked G was connected to the guard ring.

Fig. 12(a) shows the circuit used to measure I_i, the internal photovoltaic current which is used to determine Q'. The electron suppressor plate was biased 45V negative to reduce photoelectric emission from the exposed n-side of the junction. The photoelectrons which were not suppressed were eventually collected at some other surface of the grounded monochromator. Since these electrons circulated in a loop, which did not include the meter, they did not contribute to the signal. A small part of the diode case was also exposed to the incident photon flux, but the electron suppressor plate eliminated any significant photoelectric emission from it.

With the diode connected as shown in Fig. 12(b), $I_i - I_\varphi$ was measured. The n-lead was isolated from ground, and therefore the photoelectrons emitted from the diode surface flowed through the meter. The p-side of the junction was connected to ground

---

*See also Fig. 7.

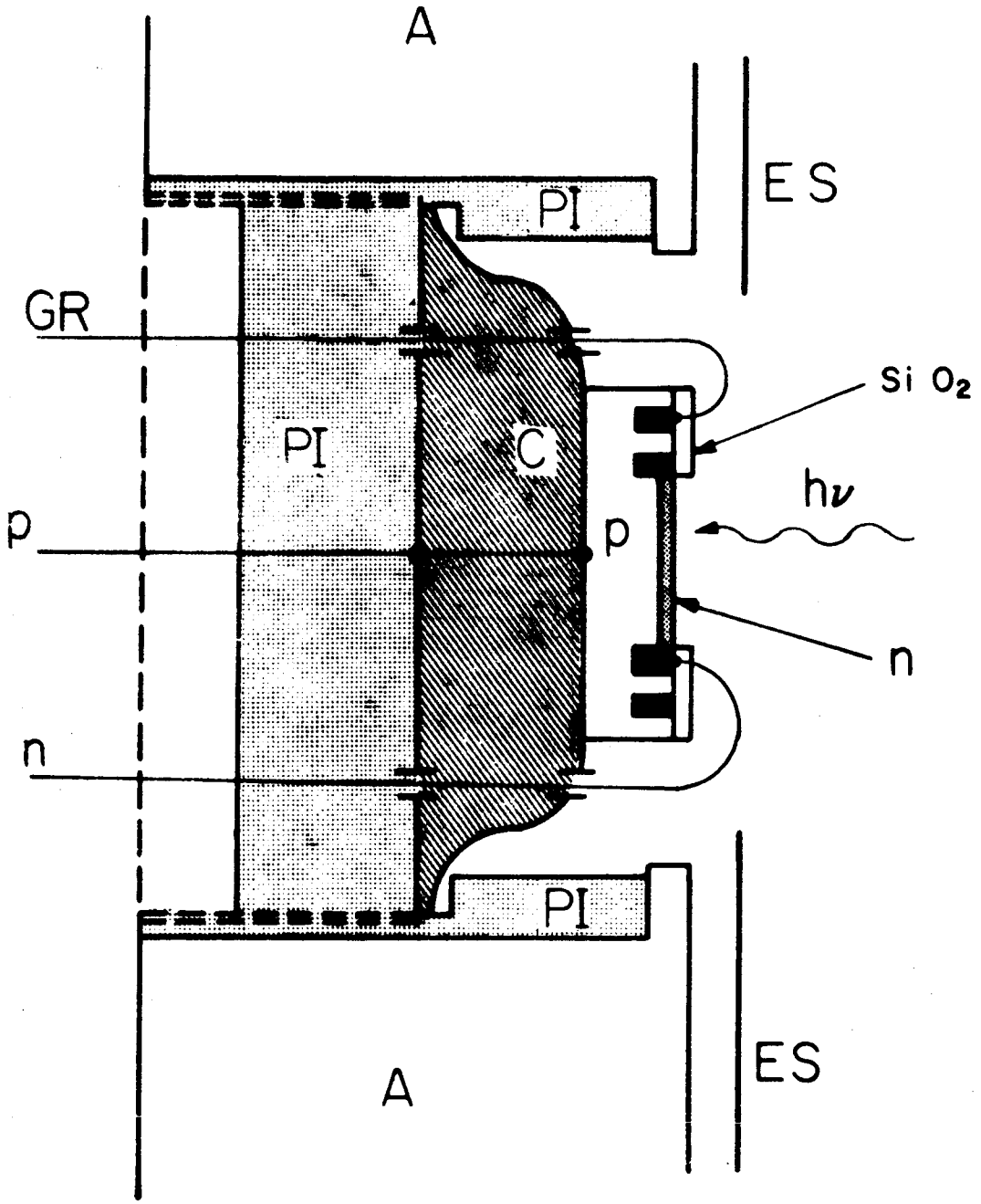

Fig. 11. Electrical Connections to Diode. The dimensions of the diode have been exaggerated, and the relative positions of the leads have been changed from the actual geometry indicated in Fig. 7 to a more convenient one to improve clarity.

A: Aluminum detector holder;
PI: Plastic insulator between diode and the holder;
ES: Electron suppressor plate;
GR: Lead to the guard ring of the diode;
C: Metal header;
p: Lead to the p-side of the diode (also indicates p-type Si);
n: Lead to the n-side of the diode (also indicates n-type Si);

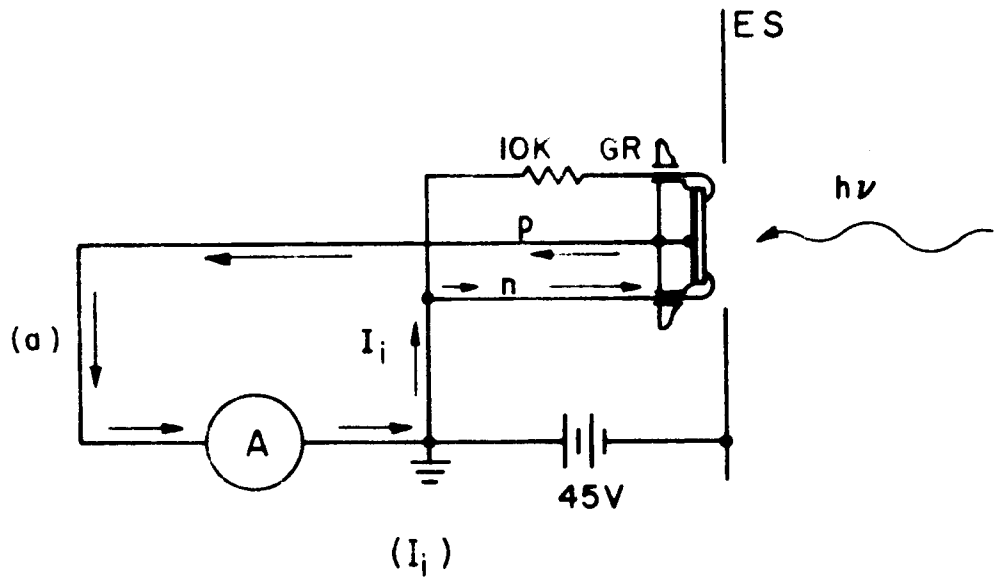

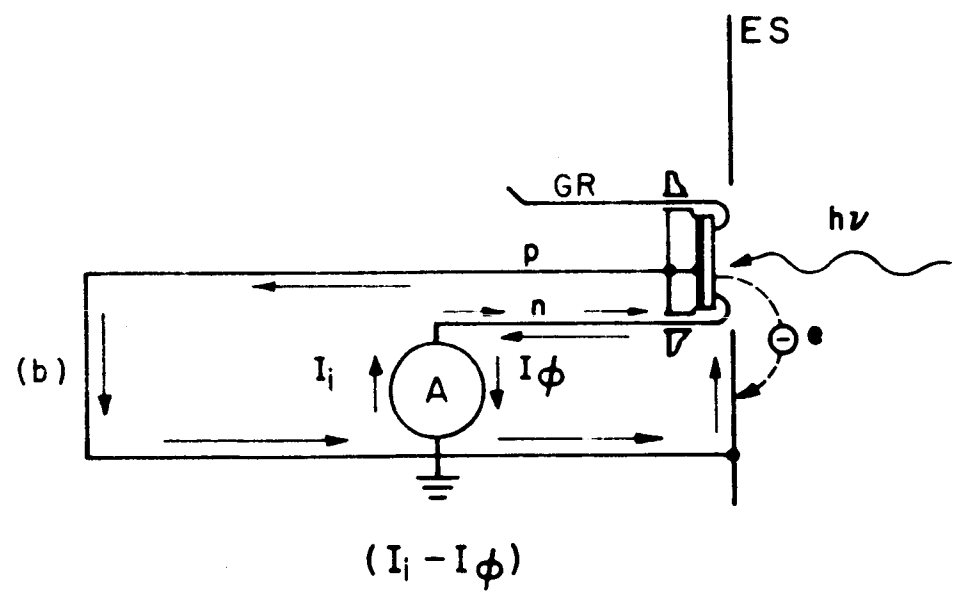

Fig. 12. Electrical Circuits Used to Make Various Measurements

(a): measured I_i, the internal photovoltaic current;
(b): measured the difference between I_i and the external photovoltaic current, I_φ;

GR: Lead to the guard ring; ES: Electron suppressor plate;
p: Lead to the p-side of diode; n: Lead to n-side of diode;
e: photoelectrons emitted from n-side of the junction and collected at ground potential (dashed arrow indicates trajectory of electron).

causing the internally generated current to flow through the meter and be detected. Photoelectrons emitted from the case of the diode were not detected since they circulated in a loop that did not include the meter.

The signals from the thermopile and the silicon junction photodiodes were all analyzed by the same synchronous amplifier-recorder system,* which consisted of five main parts: a mechanical light source chopper; a low noise, high gain ac amplifier; a twin-tee narrow band filter; a synchronous detector; and a strip chart recorder. This instrument could be operated at chopping frequencies from 5 to 200 cps, but all measurements were made with a fixed chopping frequency of 11 cps over an electrical bandwidth of 1 or 1/3 cps. There was also a built-in calibration signal which applied a known voltage across the precision input resistors. This feature guaranteed an over-all accuracy of 2 per cent on any scale. A built-in oscilloscope monitored the phase between the input and rectification signals.

The detectors were connected to various resistors in the input grid circuit according to their input impedance. The thermopile, which had a low impedance of about 20 ohms, was connected to a 1:100 step-up transformer, and the high-resistance silicon photodiodes across 1 megohm. The thermopile was calibrated using an N.B.S. irradiance standard in the usual way.[16]

---

*Manufactured by Brower Laboratories, Westboro, Mass., Model No. 103M.

[16] K. Watanabe, F. M. Matsunaga, and R. S. Jackson, J. Quant. Spectrosc. Radiat. Transfer 5, 329 (1965).

All absolute measurements were made by rotating the grating until a strong spectral line was incident on the thermopile. Its output gave the intensity of the line in terms of photons/sec. The two diodes were then moved in turn behind the exit slit and their response noted. The thermopile was again moved behind the exit slit and its second response compared with its initial response as a check on the stability of the light source. Then the grating was rotated and the procedure repeated with a new line.

V. RESULTS

Over one hundred spectral lines, from 3000 to 400Å, were observed with the silicon junction photodiodes. However, only about 25 of these were intense enough for reliable absolute photon flux measurements. The results of these measurements for 13 points from 584 to 1608Å are given in Fig. 13. A qualitative analysis of the spectra obtained with these diodes indicated no drastic changes in response at wavelengths greater than 850Å. Below 850Å the response apparently increased sharply.

Quantitative measurements were limited by the relatively low sensitivity of the calibrated thermopile. Many lines which registered clearly with the diode detectors, giving their relative sensitivity, were undetectable with the thermopile. In particular, many lines in the air spark spectrum in the 600 to 400Å region were easily detected by the diodes, Fig. 14, but could not be observed at all with the thermopile. This indicated that they were actually weak lines and that the strong signals they produced in the diodes were indicative of the high sensitivity of the diode in this region. The diode response measurements were made with the diode connected as shown in Fig. 12(a). With this connection, only the internal photocurrent contributed to the diode signal.

The sensitivity decreased slightly from 1608Å to about 850Å and then increased rapidly. The response at 584Å for diode A was 1.4 electrons per incident photon. This was a

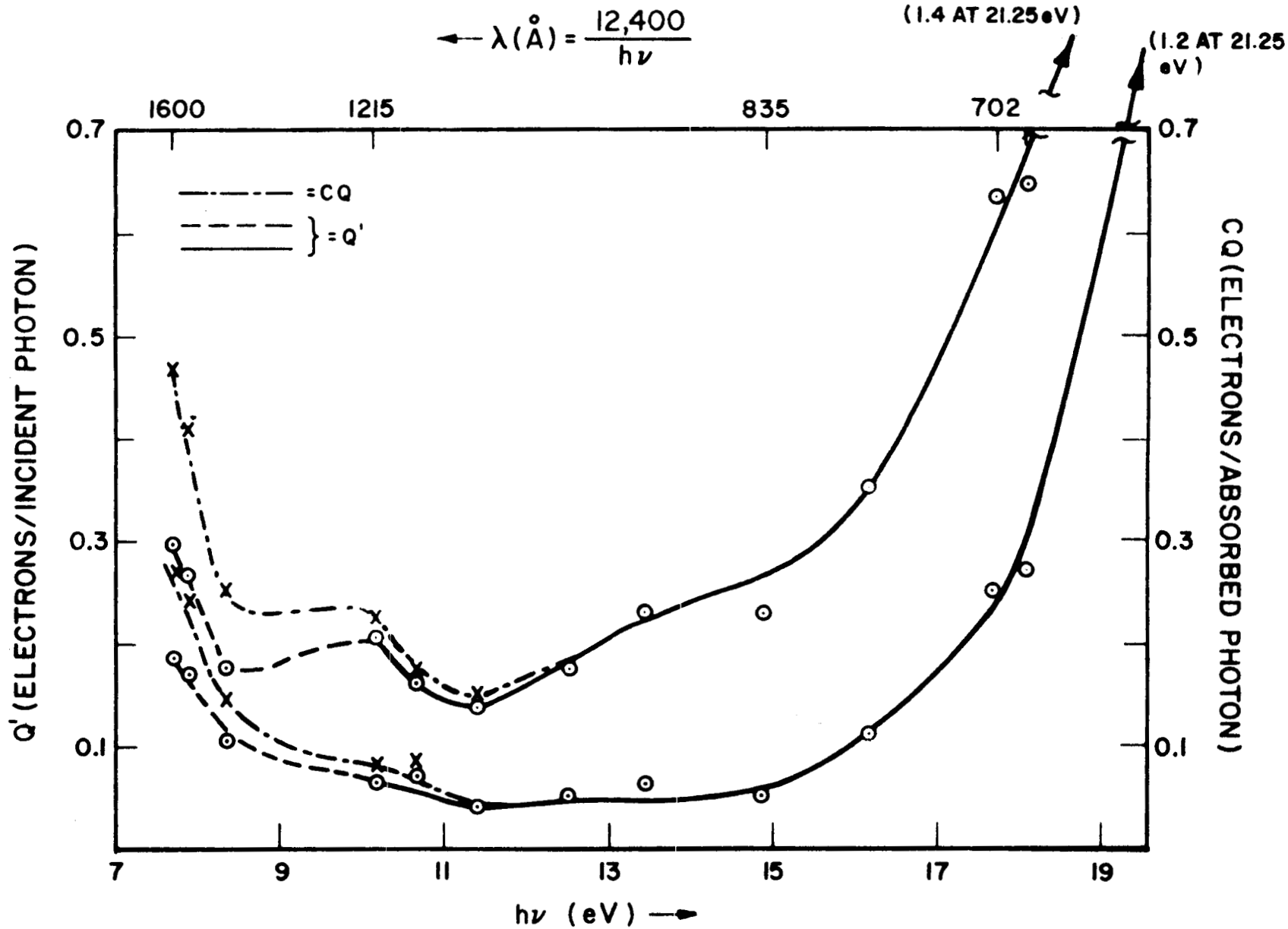

Fig. 13. Measured and Calculated Values of Diode Sensitivity. The measured value, Q', and the value calculated from it, CQ, are related by the equation Q = (1-R)CQ, where R is the reflectance of silicon.

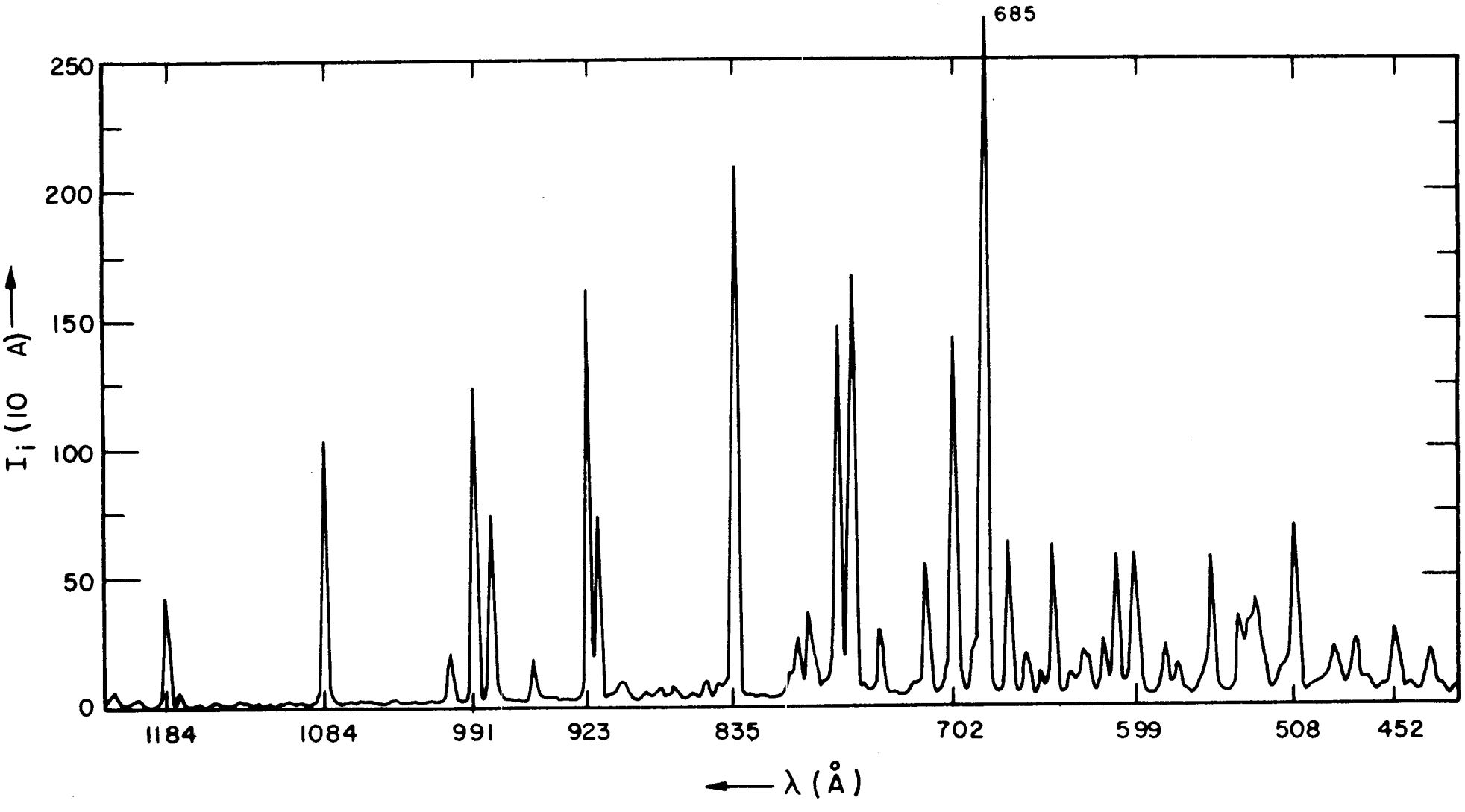

Fig. 14. Air Spark Spectrum as Resolved by a Junction Photodiode. Used in the Mode Shown in Fig. 12a.

ten fold increase over its response at 1084Å. Diode B showed a thirty fold increase over the same region, from 0.04 to 1.2 electrons per incident photon.

If the diode is connected as shown in Fig. 12(b), the internal photocurrent, I_i, measured above, is opposed by the external photoelectric current, I_φ. Fig. 15 shows an air spark trace of a diode's response in this configuration. At wavelengths greater than 1200Å, the internal photocurrent, I_i, was larger than the external photoelectric current, I_φ, and therefore the net signal was in the negative direction. This crossover point is seen clearly with a hydrogen discharge which has many lines near 1200Å. Between 1200 and 700Å, I_φ was greater than I_i, and the net signal was in the positive direction. The signal became negative again below 700Å, where I_i increased rapidly and became greater than I_φ.

These polarity reversals may be of considerable aid when identifying unfamiliar spectra, since second order lines are easily distinguished from first order ones between 2400 and 700Å. For example, 835Å in the second order appeared as a positive signal in a region where all first order lines were negative, and 510Å in the second order appeared as a negative signal in a region where all the first order lines were positive.

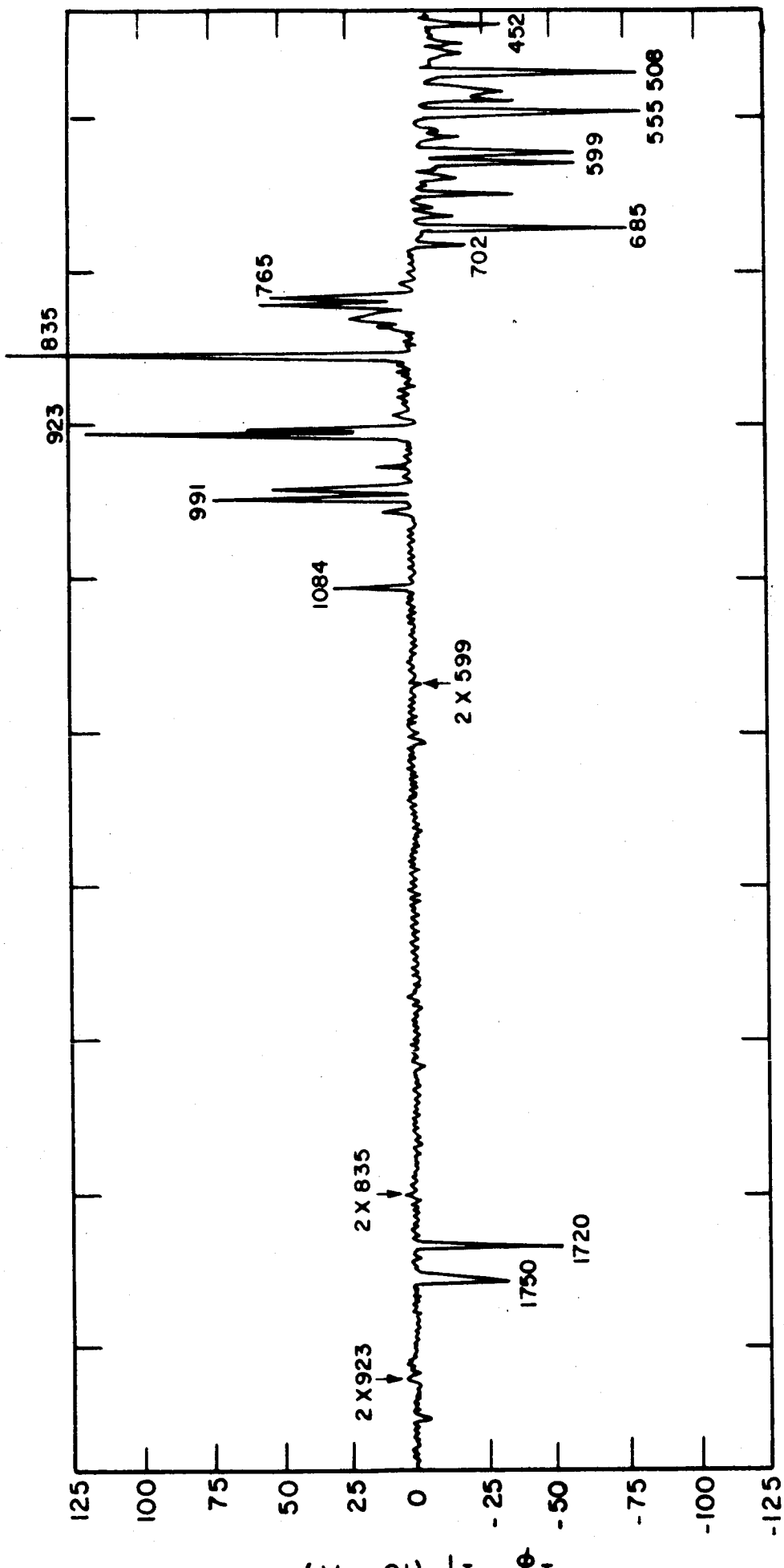

Fig. 15. Air Spark Spectrum as Resolved by a Junction Photodiode, Used in the Mode Shown in Fig. 12b. (Note that the polarity of the meter was reversed so that I_i is negative.)

VI. DISCUSSION

The results of this work are of interest from several points of view. As new detectors of extreme uv and soft x rays, the silicon junction photodiodes should play an important role in future research in this field, both in the laboratory and in space science applications. The device requires no external power supply, exhibits no significant fatigue properties, can be cycled between vacuum and air repeatedly, and possesses all the obvious advantages of a solid state sensor. High density linear arrays and mosaics of these detectors may be readily fabricated, using the state-of-the-art planar technology. The responsivity is intermediate to that of thermopile radiation detectors and sodium salicylate conversion combined with a photomultiplier. In addition, when employed in the proper mode, the photodiode is a convenient order-sorter.

The electron-hole pairs generated and separated by these junction devices as a function of photon energy is a matter of fundamental interest. One can write

$$Q' = (1 - R)CQ, \tag{9}$$

where R is the reflectance, Q the quantum efficiency of internal pair production, and C the collection efficiency discussed earlier in connection with Eq.(6). It is only for wavelengths less than 1300Å that the reflectivity correction (1 - R) is significant to a determination of Q' (Fig. 13).

Sasaki and Ishiguro[2] have extended the measurements of Philipp and Taft[1] on the absorption of silicon to photon

energy of 20 eV (Fig. 16). From 5 eV to 20 eV, the extinction coefficient, k, shows a monotonic decrease so that one would expect pair generation to occur closer to the junction plane as one proceeds to shorter wavelengths from the peak absorptions at 4.5 to 6 eV. Intuitively, and analytically from Eq.(6), one might expect a corresponding increase in C. However, it is also necessary, even in the simple model leading to Eq.(6), to take into account the variation of L_s and s with photon energy, i.e., the electron mobility may be a strong function of the conduction band branch. Loh and Phillips[7] have considered such a possibility in discussing the results of Loh[17] in the near uv.

The internal quantum efficiency of silicon has been studied by Vavilov[18] in the photon energy range from 1.5 to 4.9 eV, shown in Fig. 17. The value of Q is unity up to 3.4 eV and then rapidly increases to a value of Q = 2.1 at $h\nu$ = 4.9 eV, which he attributed to impact ionization by the energetic carriers. The threshold kinetic energy E_t for this secondary multiplication effect he estimated from this result is

$$E_t = 3.4 - E_g = 2.3 \text{ eV}$$

for E_g = 1.1 eV. According to Shockley[19] the threshold for secondary pair production should be about 2.2 eV rather than 1.1 eV since the most likely impact ionization event (greatest cross section) occurs when the available kinetic energy is

---

[17] E. Loh, J. Phys. Chem. Solids 24, 493 (1963).

[18] V. S. Vavilov, J. Chem. Phys. 8, 223 (1959).

[19] W. Shockley, Czech. J. Phys. 11, 81 (1961).

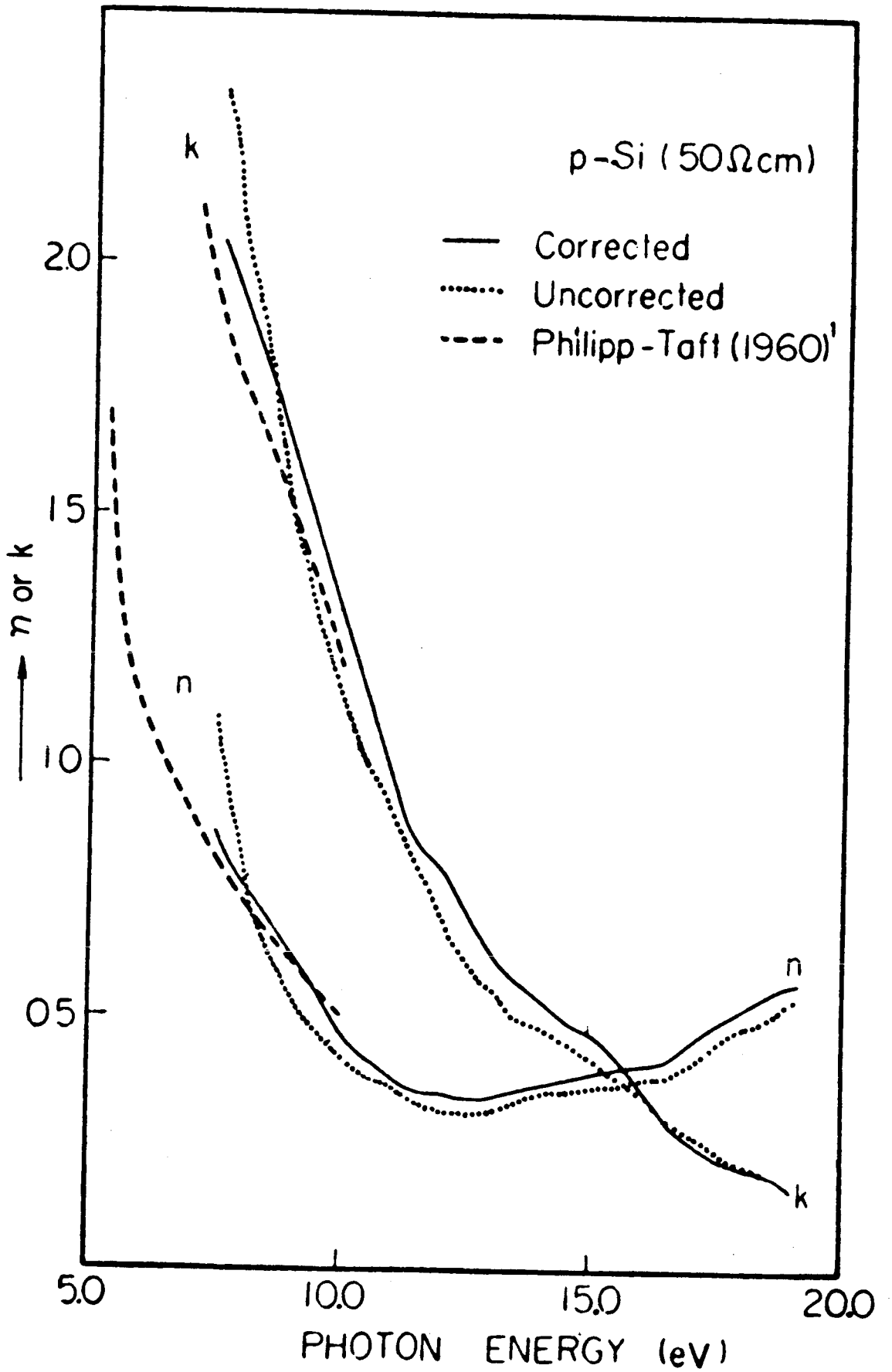

Fig. 16. Optical Constants of Silicon from hν = 5 to 20 eV. The Solid and the dotted curves are taken from Sasaki and Ishigura's work. The solid curve includes corrections for polarization.

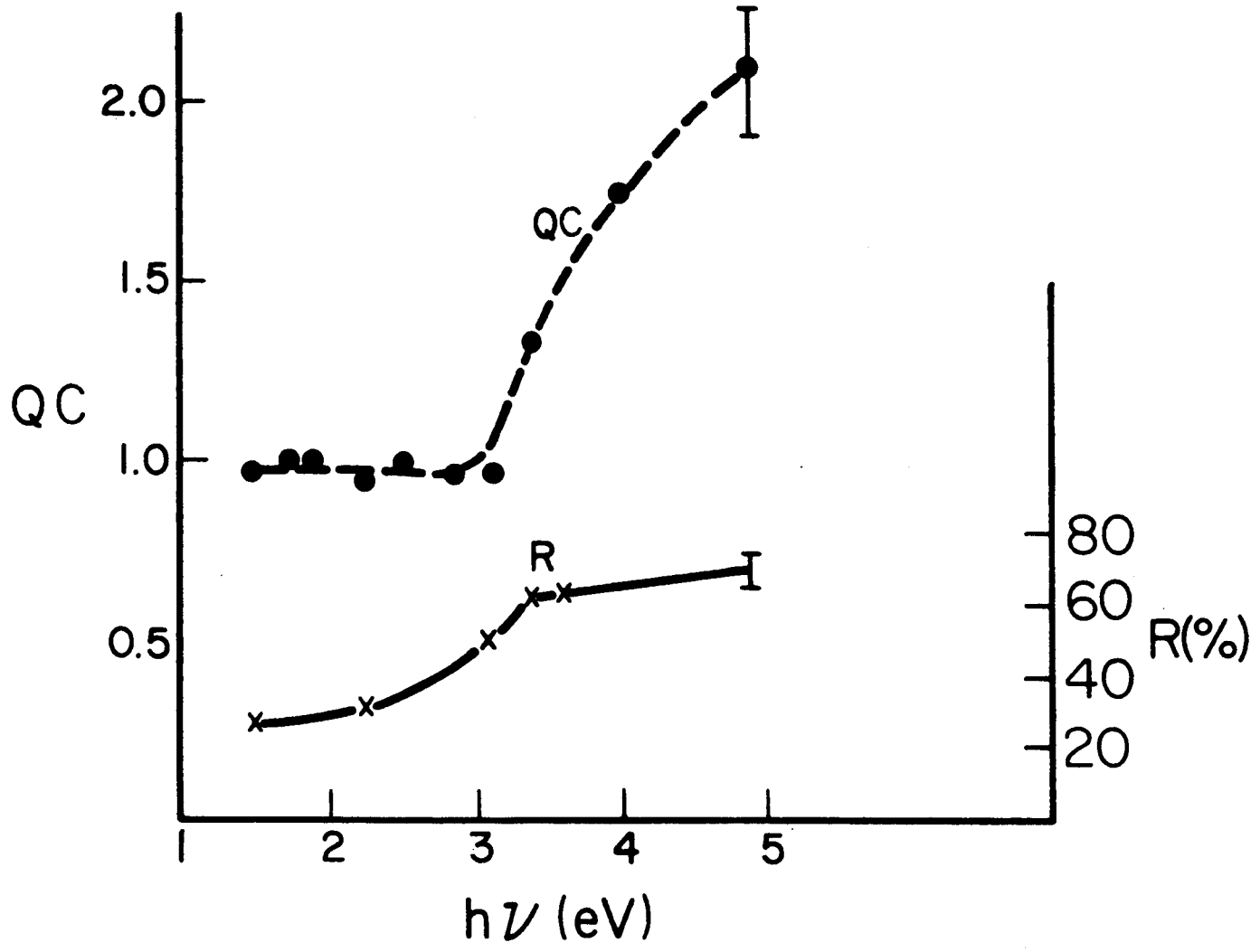

Fig. 17. Reflectance, R, and Product of Quantum Yield and Collection Efficiency, QC, for Silicon

equally partitioned between the hole and the electron.

Using a surface-barrier diode configuration in the reverse bias mode, Tuzzolino[9,10] extended the measurements of Q to 21.2 eV. His results are shown in Fig. 18.

The data presented in Fig. 13 are not consistent with the data of Tuzzolino and the model described earlier. His predicted large enhancement in QC does not appear in this work until photon energies of 18 eV are reached, while in his work the rise starts at 6 eV. Also, the apparent drop in QC observed from 6 eV to 10 eV is inconsistent with the expected increase in both Q and C. It is possible but not likely that the absorption characteristics of a highly doped n-type layer may differ considerably from the data obtained by Sasaki and Ishiguro[2] in their p-type 50 ohm-cm sample.* A measurement of the optical constants for degenerate surface layers in Si should resolve this question. The other possibility involves questions of both mobility and lifetime of carriers as a function of the photon energy. Finally, the measurement of spectral responsivity as a function of applied bias should be carried out in order to define the contribution, if any, of the diode base (p-layer). In this analysis, it has been implicitly assumed that all events of interest occur in the diffused layer $0 < x < x_J$ for photon energies in excess of 6 eV.

---

*"Reflectance Measurements from Strongly Doped n- and p-Type Silicon Crystals in the Extreme Vacuum Ultraviolet," J. Earl Rudisill, M.S. Thesis, U.S.C., May 1965.

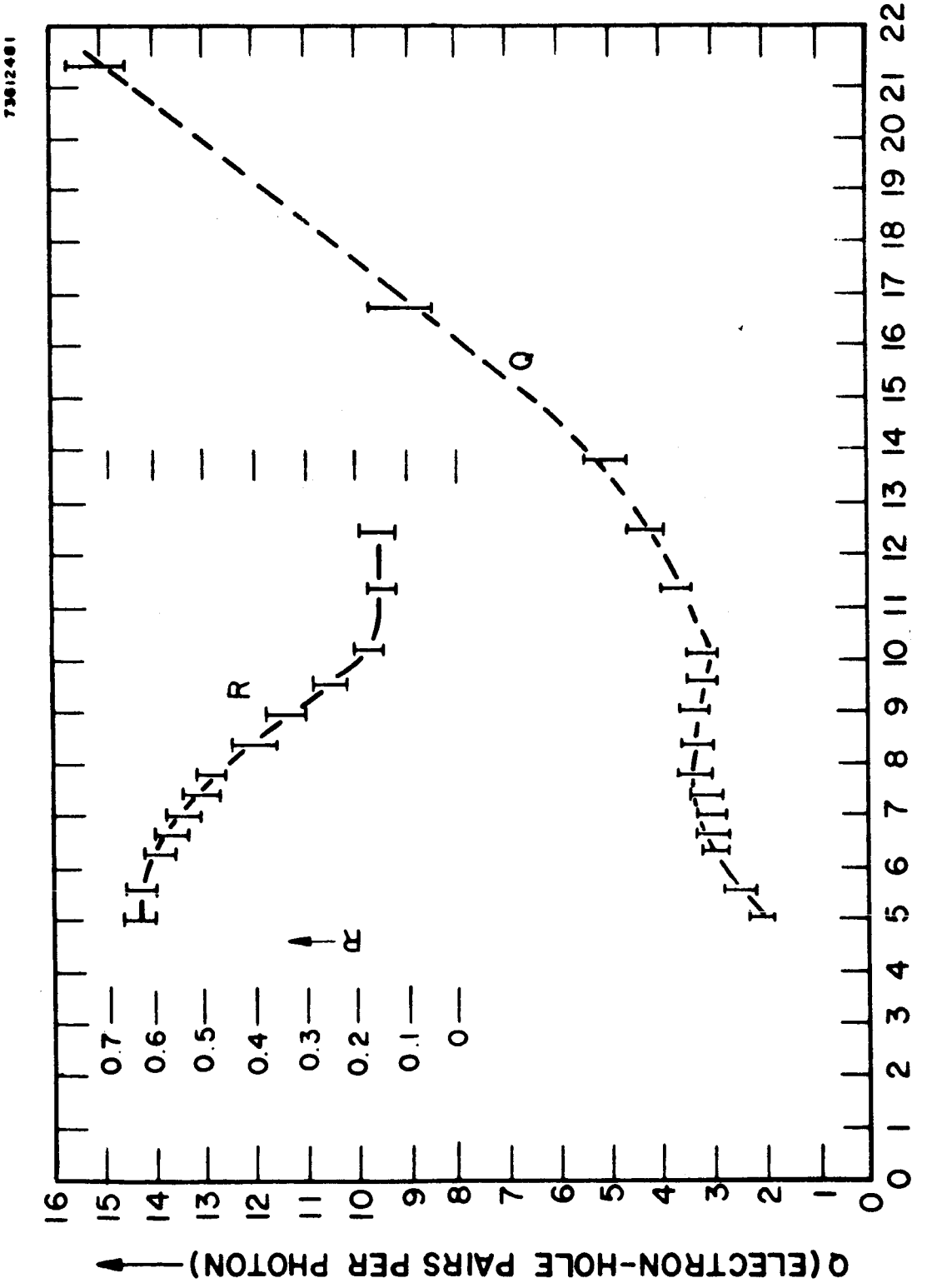

Fig. 18. Tuzzolino's Results on Far UV Response in Silicon. Results are the average reflectance and quantum efficiency for seven silicon photodiodes.